Thermodynamic and Transport Properties of $H_2/H_2O/NaB(OH)_4$ Mixtures Using the Delft Force Field (DFF/$B(OH)_4^-$)

Habibi, Parsa; Postma, Julien R.T.; Padding, Johan T.; Dey, Poulumi; Vlugt, Thijs J.H.; Moultos, Othonas A.

DOI
10.1021/acs.iecr.3c01422

Publication date
2023

Document Version
Final published version

Published in
Industrial and Engineering Chemistry Research

I&EC research
Industrial & Engineering Chemistry Research

pubs.acs.org/IECR

Article

Thermodynamic and Transport Properties of $H_2/H_2O/NaB(OH)_4$ Mixtures Using the Delft Force Field (DFF/$B(OH)_4^-$)

Parsa Habibi, Julien R. T. Postma, Johan T. Padding, Poulumi Dey, Thijs J. H. Vlugt, and Othonas A. Moultos*

Cite This: *Ind. Eng. Chem. Res.* 2023, 62, 11992−12005

Read Online

ACCESS | Metrics & More | Article Recommendations | Supporting Information

ABSTRACT: Sodium borohydride ($NaBH_4$) has a high hydrogen (H_2) gravimetric capacity of 10.7 wt %. $NaBH_4$ releases H_2 through a hydrolysis reaction in which aqueous $NaB(OH)_4$ is formed as a byproduct. $NaB(OH)_4$ strongly influences the thermophysical properties of aqueous solutions (i.e., densities, viscosities, and electrical conductivities) and the hydrolysis reaction kinetics and conversion of $NaBH_4$. Here, molecular dynamics (MD) simulations are performed to compute viscosities, electrical conductivities, and self-diffusivities of H_2, Na^+, and $B(OH)_4^-$ for a temperature and concentration range of 298−353 K and 0−5 mol $NaB(OH)_4$/kg water, respectively. Continuous fractional component Monte Carlo (CFCMC) simulations are used to compute the solubilities of H_2 and activities of water in aqueous $NaB(OH)_4$ solutions for the same temperature and concentration range. A new force field is developed (Delft force field of $B(OH)_4^-$: DFF/$B(OH)_4^-$) in which $B(OH)_4^-$ is modeled as a tetrahedral structure with a scaled charge of −0.85. The OH group in $B(OH)_4^-$ is modeled as a single interaction site. This force field is based on TIP4P/2005 water and the Madrid-2019 Na^+ force field. The MD simulations can accurately capture the densities and viscosities within 2.5% deviation from available experimental data at 298 K up to a concentration of 5 mol $NaB(OH)_4$/kg water. The computed electrical conductivities deviate by ca. 10% from experimental data at 298 K for the same concentration range. Based on the molecular simulations results, engineering equations are developed for shear viscosities, self-diffusivities of H_2, Na^+, and $B(OH)_4^-$, and solubilities of H_2, which can be used to design and model $NaBH_4$ hydrolysis reactors.

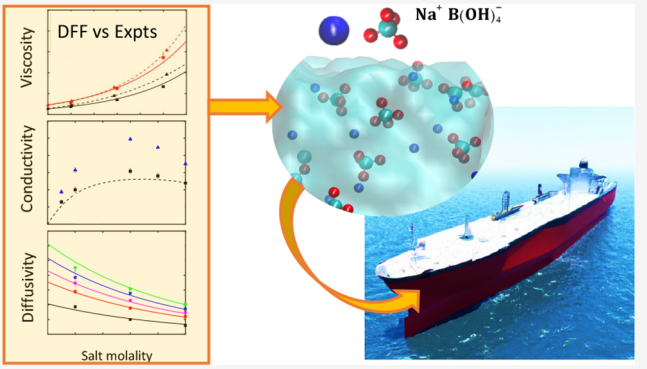

1. INTRODUCTION

Aqueous borate ions are of relevance to a wide array of industrial applications ranging from nuclear electric power to flame retardants.[1−6] The potential use of sodium borohydride ($NaBH_4$) for H_2 storage in applications such as maritime shipping, due to its high gravimetric capacity of 10.7 wt %,[7−17] has increased the interest for aqueous borate ion chemistry. The hydrolysis reaction of $NaBH_4$ produces H_2 and sodium metaborate ($NaBO_2$) according to[18,19]

$$NaBH_4 + 2H_2O \rightarrow NaBO_2 + 4H_2 \quad (R1)$$

Sodium metaborate dissolves in water forming aqueous $NaB(OH)_4$[19−21]

$$NaBO_2 + 2H_2O \rightarrow Na^+(aq) + B(OH)_4^-(aq) \quad (R2)$$

Other hydroxyl-hydrate borates such as $B(OH)_3$ and $B_3O_3(OH)_4^-$ can also be present in the aqueous phase;[19,20,22,23] however, previous experimental and theoretical studies of aqueous $NaBO_2$ solutions suggest that more than 95% of borate ions in water are in the form of $B(OH)_4^-$.[20,22] Aqueous $B(OH)_4^-$ ions are also formed when boric acid (H_3BO_3), which acts as a Lewis acid, dissolves in water.[24−26] The dissolution of borates in water is discussed in detail in refs 22−24, 27. In this work, only hydroxyl-hydrate borate ions of the type $B(OH)_4^-$ are considered.

The solubility limit of $NaBO_2$ at 298 K is 4.25 mol $NaBO_2$/kg water,[28−30] which corresponds to a solubility of 5.02 mol $NaB(OH)_4$/kg water based on reaction R2. At the solubility limit (at 298 K), the viscosity of the aqueous $NaB(OH)_4$ solution is ca. 6 times higher than that of pure water.[21] The presence of $NaB(OH)_4$ has a significant influence on the thermophysical properties (e.g., electrical conductivities, viscosities, and densities) of the solution[21] and influences the reaction rates of $NaBH_4$ hydrolysis.[31−33] Uncontrolled crystallization of $NaB(OH)_4$ is one of the major concerns in

Received: April 28, 2023
Revised: July 1, 2023
Accepted: July 6, 2023
Published: July 22, 2023

$NaBH_4$ hydrolysis reactors.[29,34,35] Detailed knowledge of the thermophysical properties of aqueous $NaB(OH)_4$ will help in modeling the crystallization rates and the design of $NaBH_4$ hydrolysis reactors.

The densities, viscosities, and electrical conductivities of aqueous $NaB(OH)_4$ solutions (0−5 mol $NaB(OH)_4$/kg water) at 298 and 323 K have been measured experimentally by Zhou et al.[21] To the best of our knowledge, thermophysical properties of aqueous $NaB(OH)_4$ solutions at temperatures higher than 323 K are not available, despite being relevant for $NaBH_4$ hydrolysis reactors, which usually operate at 298−363 K.[36−38] Data on the solubilities of H_2 and the self-diffusivities of H_2, Na^+, and $B(OH)_4^-$ in $NaB(OH)_4$ solutions are also not available even though H_2 mass transfer[31] and $NaB(OH)_4$ crystallization[29,34,35] are crucial for optimizing the performance of $NaBH_4$ hydrolysis reactors. Molecular simulation, specifically molecular dynamics (MD) and Monte Carlo (MC) simulations, provides a complementary approach to experiments for investigating thermophysical properties that are difficult to measure experimentally[39−43] (i.e., self-diffusivities of ions and H_2) at elevated temperatures (ca. 353 K) and salt molalities (ca. 5 mol $NaB(OH)_4$/kg water). MD or MC simulations of aqueous $NaB(OH)_4$ require force fields that are either based on ab-initio calculations or parameterized based on existing experiments.[44,45] Zhou et al.[20] have used ab-initio simulations and empirical potential structure refinement (EPSR) to investigate the structure and hydration of aqueous $NaB(OH)_4$. The EPSR potential of Zhou et al.[20] can accurately model radial distribution functions (RDFs) and the hydration numbers of the ions; however, it is not parameterized for viscosities and electrical conductivities of the solution. Despite the significant influence of the $NaB(OH)_4$ concentration on the transport properties of the solution,[21] no attempts have been made to develop a classical $B(OH)_4^-$ force field that can describe and predict the densities, viscosities, and electrical conductivities of $NaB(OH)_4$ solutions.

In this work, we propose a new classical force field for $B(OH)_4^-$ (the so-called Delft force field for $B(OH)_4^-$, which will be referred to hereafter as DFF/$B(OH)_4^-$), which combined with TIP4P/2005 water[46] and the Madrid-2019 Na^+ force field[47] can accurately model densities and viscosities of $NaB(OH)_4$ solutions with a maximum deviation of 2.5% from experimental results up to the solubility limit at 298 K. $B(OH)_4^-$ is modeled as a tetrahedral structure with a scaled net charge of −0.85. The OH group in $B(OH)_4^-$ is modeled as a single interaction site. DFF/$B(OH)_4^-$ is an addition to the Delft force field family (see our work on the DFF/OH^-[41]). The computed electrical conductivities of aqueous $NaB(OH)_4$ solutions using the DFF/$B(OH)_4^-$ at 298 and 323 K are within 10% of available experimental data. The densities, viscosities, and self-diffusivities of H_2, Na^+, and $B(OH)_4^-$ in aqueous $NaB(OH)_4$ solutions at 298−353 K and 0−5 mol $NaB(OH)_4$/kg water are computed using MD simulations. The solubilities of H_2 and activities of water in aqueous $NaB(OH)_4$ solution for the same temperature and concentration range are computed using continuous fractional component Monte Carlo (CFCMC)[48−50] simulations. To allow for simple extraction of the computed properties, engineering equations are developed by us.[40,41] All the computed viscosities of aqueous $NaB(OH)_4$ solutions, self-diffusivities for H_2, Na^+, and $B(OH)_4^-$, and the solubilities of H_2 are fitted to empirical equations, which can be used to model $NaBH_4$ hydrolysis reactors.

This paper is organized as follows: In Section 2, the force fields used for H_2O, Na^+, and H_2 are presented and the details for the MD and CFCMC simulations[48−50] are explained. In Section 3.1, a force field for $B(OH)_4^-$ is developed based on experimental densities, viscosities, and RDFs of aqueous $NaB(OH)_4$ at 298 K and 1 bar. The computed densities and viscosities for a temperature range of 298−353 K are discussed in Section 3.2. The electrical conductivities and the self-diffusivities of ions are reported in Section 3.3. The self-diffusivities of H_2, solubilities of H_2, and activities of water in aqueous $NaB(OH)_4$ solutions are discussed in Sections 3.4 and 3.5. Our conclusions are outlined in Section 4.

2. METHODOLOGY

2.1. Force Fields. Lennard-Jones (LJ) and electrostatic interactions are used to model interatomic interactions. H_2O is modeled using the four-site rigid TIP4P/2005[46] force field. This water force field can accurately capture the densities, self-diffusivities, and viscosities of pure H_2O and H_2O solutions (e.g., aqueous NaCl,[40,47] KCl,[47] NaOH, and KOH[41]) for a wide range of conditions.[42,51−55] For Na^+ ions, the Madrid-2019[47] and Madrid-Transport[56] force fields are used. Both Madrid Na^+ force fields are non-polarizable force fields, which make use of scaled charges.[47,56] In non-polarizable models, charges of ions in water and for ionic liquids are commonly scaled down.[47,56,57] In the Madrid-2019[47] and Madrid-Transport[56] model, the charges of Na^+ ions are scaled down to 0.85 and 0.75, respectively. This charge scaling leads to more accurate viscosity predictions for aqueous electrolyte solutions (e.g., NaCl and Na_2SO_4) compared to using unscaled charges.[47] The use of scaled charges is discussed in detail in refs 47, 56, 57. The three-site Marx[58] model is used for computing the H_2 solubilities and self-diffusion coefficients. Analytic tail corrections for the LJ interactions are applied for computing energies and pressures. The $B(OH)_4^-$ force field is developed in this work and is discussed in Section 3.1. All force field parameters for H_2O, Na^+, and H_2 are listed in Tables S1−S3 of the Supporting Information. All molecules and ions are considered rigid. The Lorentz−Berthelot mixing rules[44,45] are used with the exception of [Na^+/$B(OH)_4^-$−H_2O] LJ interactions as specified in Tables 1 and S3.

2.2. MD Simulations. MD simulations are carried out using the open-source large-scale atomic/molecular massively parallel simulator (LAMMPS)[59] (version August, 2018). Sample LAMMPS input files are provided as Supporting Information and can also be downloaded from here: https://github.com/omoultosEthTuDelft/B-OH-4—Delft-Force-Field-. Rigid body constraints are applied to all molecules.[60] The Verlet algorithm is used to integrate Newton's equations of motion with a time step of 1 fs.[61] The particle−particle particle−mesh (PPPM)[44,62] method is used (relative error of 10^{-5}) for long-range electrostatic interactions. The PPPM method is numerically efficient and suitable for large systems (i.e., ca. 10^3 point charges or more).[63,64] A cutoff radius of 10 Å is used for LJ and the real space contribution of the PPPM method for electrostatic interactions. Periodic boundary conditions are imposed in all directions. The Nosé−Hoover thermostat and barostat[44,65,66] are applied, with coupling constants of 100 and 1000 fs, respectively. The modifications proposed by Kamberaj[67] for the Nosé-Hoover algorithm of rigid bodies are used in LAMMPS.

The OCTP plugin[68] is used to compute RDFs, self-diffusion coefficients of all species (i.e., H_2O, Na^+, $B(OH)_4^-$, and H_2),

https://doi.org/10.1021/acs.iecr.3c01422
Ind. Eng. Chem. Res. 2023, 62, 11992−12005

Table 1. Force Field Parameters for $B(OH)_4^-$ [a]

$B(OH)_4^-$ force field	q_{OH}/[e]	q_B/[e]	$q_{B(OH)_4}$/[e]	$\sigma_{(OH)(OH)}$/[Å]	$\sigma_{(OH)(Ow)}$/[Å]
V1	-0.65	1.75	-0.85	2.75	2.91
V2	-0.75	2.15	-0.85	2.85	2.96
V3	-0.85	2.65	-0.75	2.95	3.01
V4 (DFF/$B(OH)_4^-$)	-0.85	2.55	-0.85	2.95	3.01

[a]OH is modeled as a single site with a charge of q_{OH}. The B atom has a charge of q_B and is not a LJ site as it is surrounded by four OH. $q_{B(OH)_4}$ is the total charge of $B(OH)_4^-$ and is based on the scaled charges used in Madrid-2019 (0.85)[47] and Madrid-Transport (0.75).[56] $\epsilon_{(OH)(OH)}$ is the LJ energy parameter for OH−OH interactions and is equal to $\epsilon_{(OH)(OH)}/k_B$ = 50.32 K. $\sigma_{(OH)(OH)}$ and $\sigma_{(OH)Ow}$ are the LJ size parameters for OH−OH and OH−O_w (O of water) interactions. For $\epsilon_{(OH)Ow}$, $\epsilon_{(OH)Na^+}$, and $\sigma_{(OH)Na^+}$ the Lorentz−Berthelot mixing rules[44,45] are used. The V4 force field is recommended as it leads to the best agreement with experimental densities and viscosities of aqueous $NaB(OH)_4$ solutions compared to the V1−V3 force field. The parameters of the new DFF/$B(OH)_4^-$ are the ones of V4.

Onsager coefficients,[69] and the viscosities of the solutions using Einstein relations. For all details of the OCTP plugin, the reader is referred to ref 68. For each state point (temperature, pressure, and salt molality), the volume of the simulation box is obtained using a 5 ns equilibration run (*NPT* ensemble) and a consequent 5 ns production run (*NPT* ensemble), in which the average volume is computed. The average volume computed in *NPT* simulations is used in subsequent *NVT* simulations to compute transport properties and radial distribution functions (RDFs). In the *NVT* ensemble, an equilibration run of 1 ns and a production run of 20−50 ns is used. All self-diffusivities shown here are corrected for finite-size effects using the Yeh−Hummer equation.[70−73] Dynamic viscosities computed using MD are not subject to finite-size effects.[69,72,74,75] The electrical conductivities (κ) in this work are computed using the Einstein−Helfand approach.[76,77]

$$\kappa = \frac{e^2 N}{V k_B T} \sum_{i,j} z_i z_j \Lambda_{ij} \tag{1}$$

where e is the elementary charge, N is the total number of molecules, V is the volume of the simulation box, k_B is the Boltzmann factor, and T is the absolute temperature. z_i and z_j are the charges of ions of type i and j, respectively. It is important to note that z_i represents the ionic charge of the component, e.g., for Na^+ it would be 1. This means that if scaled charges are used in the force field, z_i remains unaffected. Λ_{ij} is the Onsager coefficient between ions of type i and j,[78−80] which is defined here as[69]

$$\Lambda_{ij} = \frac{1}{N} \lim_{t\to\infty} \frac{1}{6t} \left\langle \left(\sum_{k=1}^{N_i} \sum_{l=1}^{N_j} [\mathbf{r}_{k,i}(t) - \mathbf{r}_{k,i}(0)] \cdot [\mathbf{r}_{l,j}(t) - \mathbf{r}_{l,j}(0)] \right) \right\rangle \tag{2}$$

where t is time, N_i is the number of ions of type i, N_j is the number of ions of type j, and $\mathbf{r}_{k,i}(t)$ is the position vector of the k-th ion of type i at time t. The exact electrical conductivities including ion−ion correlations are computed using eq 1. For dilute electrolyte solutions, the electrical conductivities can be approximated using the Nernst−Einstein (NE) equation (κ_{NE}), which neglects ion−ion correlations:[81]

$$\kappa_{NE} = \frac{e^2}{V k_B T} \sum_i N_i z_i^2 D_i \tag{3}$$

where D_i is the self-diffusivity of ion i.

MD simulations are carried out in systems consisting of 1000 H_2O molecules and 0−90 Na^+ and $B(OH)_4^-$ ions, depending on the molality. Two H_2 molecules are added to these systems to compute self-diffusivities of H_2 in aqueous $NaB(OH)_4$ solutions. The exact number of species used for every state point is provided in Table S4 of the Supporting Information. The simulations are carried out at 298, 323, 343, and 353 K and 1 bar. For each temperature and molality, five independent simulations are carried out, each starting with a different set of initial velocities. Based on these five independent simulations, a mean and a standard deviation for densities, viscosities, self-diffusivities, and electrical conductivities are obtained. All initial configurations are created using the PACKMOL software (v20.3.1).[82] All the raw data for densities, viscosities, and self-diffusivities of H_2, Na^+, and $B(OH)_4^-$ in aqueous $NaB(OH)_4$ solutions are listed in Table S6 of the Supporting Information. The DelftBlue supercomputer[83] is used for performing MD simulations.

2.3. CFCMC Simulations. To compute the solubilities of H_2 and the activity coefficients of H_2O in aqueous $NaB(OH)_4$ solutions, CFCMC simulations are carried out using the open-source BRICK-CFCMC software package.[84,85] Sample BRICK-CFCMC input files are provided as Supporting Information and can also be downloaded from here: https://github.com/omoultosEthTuDelft/B-OH-4—Delft-Force-Field-. All simulations are carried out in the continuous fractional component[48−50] isobaric-isothermal (CFCNPT) ensemble. The methodology used to compute solubilities of H_2 follows from refs 40, 41. The MC simulation boxes are cubic, and periodic boundary conditions are applied in all directions. The simulation boxes consist of 300 water molecules and 0−27 molecules of $NaB(OH)_4$, depending on the molalities of the solution (ranging from 0 to 5 mol $NaB(OH)_4$/kg water). The exact numbers of $NaB(OH)_4$ molecules and the corresponding molalities are provided in Table S5 of the Supporting Information. To investigate finite-size effects, the solubility of H_2 is also computed in a system with 450 H_2O molecules. The computed solubility of H_2 for a system with 450 H_2O molecules is within the error bars of the computed solubility for a system with 300 H_2O molecules. Finite-size effects of MC simulations can be prominent in sub-critical conditions but are usually very small far from the critical point of the solvent.[86] Therefore, the finite-size effects of MC simulations are not considered further in this work. The Ewald summation with a relative precision of 10^{-6} is used for the long-range electrostatic interactions.[44] As the MC simulations have a smaller system size than the MD simulations, a more accurate relative precision is used, i.e., 10^{-6} versus 10^{-5}. A damping parameter (α) of 0.38 $Å^{-1}$ is used, and the number of vectors in each direction (k_{max}) is set to 8 for the Ewald summation. A cutoff radius of 10 Å is used for LJ and the real space contribution of the Ewald summation for electrostatic interactions. More details on the implementation of Ewald summation in BRICK-CFCMC can be found in the Supporting Information of ref. 84 The solubilities of H_2

https://doi.org/10.1021/acs.iecr.3c01422
Ind. Eng. Chem. Res. 2023, 62, 11992−12005

and the activity coefficients of H_2O are evaluated at 298, 323, and 353 K for a H_2 partial pressure of 1 bar.

To compute the solubilities of H_2 and the activity coefficients of H_2O, the excess chemical potentials of H_2 and H_2O (ideal gas reference state[48]) in the aqueous phase is needed. To find the excess chemical potential of H_2 and H_2O, a so-called fractional molecule of H_2 and H_2O is introduced. Fractional molecules have their interactions scaled by a continuous order parameter λ, such that at $\lambda = 0$, the molecule behaves as an ideal gas, while at $\lambda = 1$, it is fully interacting (i.e., like a "whole" or normal molecule) with its environment. Details of fractional molecules and the λ parameter are discussed in depth in refs 48−50, 84. To compute the probability of occurrence for different λ values, a histogram of 100 bins is created. A biasing function for λ ($W(\lambda)$) is created using the Wang−Landau algorithm.[87,88] The biasing function ensures a flat observed probability distribution of λ and avoids sampling issues due to energy barriers in λ-space. The Boltzmann probability distribution of λ (p_B (λ)) can be obtained from the observed probability distributions of λ (p_{obs} (λ)) and $W(\lambda)$ using[40,41,48]

$$p_B(\lambda) = \frac{\langle p_{obs}(\lambda)\exp[-W(\lambda)]\rangle}{\langle \exp[-W(\lambda)]\rangle} \tag{4}$$

in which the brackets define ensemble averages. The excess chemical potentials (μ^{ex}) of H_2 and H_2O (ideal gas reference state) are related to $p_B(\lambda)$ using[40,41,48]

$$\mu^{ex} = -k_B T \ln \frac{p_B(\lambda = 1)}{p_B(\lambda = 0)} \tag{5}$$

p_B ($\lambda = 1$) and p_B ($\lambda = 0$) are the Boltzmann probabilities of λ for $\lambda = 1$ and $\lambda = 0$, respectively.[40,41,48] The solubilities of H_2 are computed using Henry coefficients (H_{H_2}). In this work, Henry coefficients are defined using[40,41]

$$H_{H_2} = \lim_{f_{H_2}\to 0} \frac{f_{H_2}}{c_{H_2}/c_0} \tag{6}$$

where f_{H_2} is the fugacity of H_2 , c_{H_2} is the solubility of H_2 (in mol/L), and c_0 is a reference concentration set to 1 mol/L. As the solubilities of H_2 are computed at H_2 partial pressure of 1 bar, it is safe to assume that the fugacity coefficient of H_2 at these conditions is 1. The Henry coefficient is related to the excess chemical potential of H_2 using[41]

$$H_{H_2} = c_0 RT \exp\left[\frac{\mu^{ex}_{H_2}}{k_B T}\right] \tag{7}$$

where R is the gas constant. As the solubility of H_2 in water is very low (mole fraction of ca. 10^{-5} H_2 at a H_2 partial pressure of 1 bar[40,41,89]), it is assumed that the excess chemical potential of H_2 can be computed at infinite dilution using a single fractional molecule of H_2. The mole fractions of H_2 (x_{H_2}) in aqueous $NaB(OH)_4$ solutions are computed using

$$x_{H_2} = \frac{c_{H_2}\langle V\rangle}{n_{H_2O} + n_{NaB(OH)_4} + c_{H_2}\langle V\rangle} \tag{8}$$

where $\langle V\rangle$ is the average volume of the simulation box computed in the CFCNPT ensemble. n_{H_2O} and $n_{NaB(OH)_4}$ are the number of moles of H_2O and $NaB(OH)_4$ molecules in the simulation box, respectively.

The activity coefficient of H_2O (γ_m) at a molality m of $NaB(OH)_4$ can be computed using the excess chemical potential of pure H_2O ($\mu^{ex}_{H_2O,0}$) and in solution ($\mu^{ex}_{H_2O,m}$) according to[90]

$$\gamma_m = \frac{\langle \rho_w\rangle}{x_w\langle \rho_{w,0}\rangle}\exp\left[\frac{\mu^{ex}_{H_2O,m} - \mu^{ex}_{H_2O,0}}{k_B T}\right] \tag{9}$$

where $\langle \rho_w\rangle$ and $\langle \rho_{w,0}\rangle$ are the number density of H_2O molecules in a solution with a molality m $NaB(OH)_4$ and in the pure H_2O solution, respectively. x_w is the mole fraction of H_2O in the aqueous solution. $\mu^{ex}_{H_2O,m}$ and $\mu^{ex}_{H_2O,0}$ are the excess chemical potentials of H_2O in a solution with a molality m $NaB(OH)_4$ and in the pure H_2O solution, respectively. The activity of water (a_w) can be computed by multiplying the activity coefficient and mole fraction of water, i.e., $a_w = \gamma_m \times x_w$. To compute $[\mu^{ex}_{H_2O,m} - \mu^{ex}_{H_2O,0}]$ accurately, long simulations are required.[89] For all simulations, 5×10^5 equilibration cycles are carried out followed by 1.5×10^6 production cycles. A cycle refers to N trial moves, with N corresponding to the total number of molecules, with a minimum of 20. For each state point (concentration, temperature, and pressure), 100 independent simulations are performed. The Boltzmann probability distributions are averaged from blocks of 20 simulations to obtain five independent Boltzmann probability distributions for lambda of H_2O and H_2 , from which the uncertainties are estimated. MC simulations are performed serially. Performing 20 independent simulations and averaging the final Boltzmann distributions eliminate the computationally less favorable case of running a long simulation on a single processor. For all averaged distributions, the excess chemical potentials, activities of H_2O, and solubilities of H_2 are calculated to obtain a mean value and the standard deviation of the five independent blocks. Trial moves are selected with the following probabilities: 1% volume changes, 35% translations, 29% rotations, 25% λ changes, and 10% reinsertions of fractional molecules at random locations inside the simulation box. The maximum displacements for volume changes, molecule translations, rotations, and λ changes are adjusted to obtain an acceptance probability of ca. 50%. The details of the trial moves are described in refs 84, 85. All the raw data for excess chemical potentials of H_2 and H_2O, the solubilities of H_2, and the activities of H_2O in aqueous $NaB(OH)_4$ solutions are listed in Table S7 of the Supporting Information.

3. RESULTS AND DISCUSSION

3.1. $B(OH)_4^-$ Force Field Development. To compute the diffusivities of H_2 and ions (Na^+, $B(OH)_4^-$) in aqueous $NaB(OH)_4$ solutions, a force field for $B(OH)_4^-$ is required, which can accurately model the experimental densities (maximum of 2.5% deviation) and viscosities (maximum of 5% deviation) of aqueous $NaB(OH)_4$ solution. To the best of our knowledge, no $B(OH)_4^-$ force field is available for this purpose. In this work, the OH group of $B(OH)_4^-$ is modeled using a single interaction site (i.e., H is modeled implicitly, contrary to the DFF/OH^- in which O and H are two distinct sites[41]). $B(OH)_4^-$ is a tetrahedral structure with the B atom in the center (OH−B−OH angle of 109.5°) as shown in Figure 1. The bond length between B and OH is set to 1.49 Å, which

https://doi.org/10.1021/acs.iecr.3c01422
Ind. Eng. Chem. Res. 2023, 62, 11992−12005

equals the bond length between B and O as reported in a prior density functional theory study of aqueous $NaB(OH)_4$.[20]

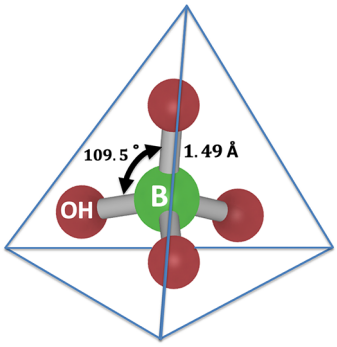

Figure 1. $B(OH)_4^-$ is modeled as a rigid tetrahedral structure (OH−B−OH angle of 109.5 °) with a single interaction site for OH. The B−(OH) bond length in this model equals 1.49 Å, which is the computed bond length between B−O reported in a prior density functional theory study of aqueous $NaB(OH)_4$ by Zhou et al.[20] iRASPA is used for this visualization.[91]

This $B(OH)_4^-$ force field is parameterized based on the TIP4P/2005 water model.[46] There are two distinct interaction sites in $B(OH)_4^-$ (i.e., $(OH)^{\delta-}$ and $B^{\delta+}$), and the total charge is equal to $q_{B(OH)_4} = q_B + 4 \times q_{(OH)}$. The total charge of $B(OH)_4^-$ matches the charge of Na^+ such that $q_{B(OH)_4} + q_{Na} = 0$. In this work, the charge distribution (i.e., q_B and $q_{(OH)}$) is considered as an additional degree of freedom to obtain accurate densities and viscosities for aqueous $NaB(OH)_4$ solutions. As such the force fields developed in this work should not be used to compute the octupole moment of the $B(OH)_4^-$ structure, which depends on the charge distribution inside the ion.[92,93] The B atom in $B(OH)_4^-$ is not an LJ site as it is surrounded by four OH groups. Two different Na^+ force fields are considered, i.e., the Madrid-2019[47] (q_{Na} = 0.85) and the Madrid-Transport[56] (q_{Na} = 0.75). Other than having different charges, these two Na^+ force fields have different cross interaction parameters with the TIP4P/2005 water force field.[46] The complete details of these force fields can be found in Table S3 of the Supporting Information. For each Na^+ force field, ca. 900 different $B(OH)_4^-$ models are created with varying LJ parameters for the OH group and charge distributions (i.e., different values of q_B and q_{OH}). The LJ parameter ranges and grid, and the charge distributions are discussed in Figure S1 of the Supporting Information. As shown in Figure S1, for all these models, the deviation of computed density versus the experimental density is evaluated at 5 mol $NaB(OH)_4$/kg water at 298 K and 1 bar. Based on these simulations, four different versions of the $B(OH)_4^-$ force field are probed (e.g., V1−V4) and listed in Table 1, which accurately model experimental densities with a maximum deviation of 2.5%. Different charge distributions (i.e., $q_{(OH)}$ and q_B) are used for the V1−V4 models. These different charge distributions are probed to investigate which $B(OH)_4^-$ force field can accurately model both the densities and viscosities of aqueous $NaB(OH)_4$ solutions. V1, V2, and V4 have a total charge of −0.85 and are based on the Madrid-2019 Na^+ force field.[47] V3 has a total charge of −0.75 and is combined with the Madrid-Transport Na^+ force field.[56] Details of the four different versions of the $B(OH)_4^-$ model during the force field development phase are listed in Table 1.

Figure 2 shows the computed densities and viscosities as functions of the $NaB(OH)_4$ molality for the V1−V4 models at 298 K and 1 bar. The experimental data of Zhou et al.[21] at the same conditions are also shown in Figure 2 as dashed lines. Based on Table 1, it can be observed that $B(OH)_4^-$ models with larger absolute values of q_{OH} and q_B (comparison between V1, V2, and V4) require larger values of $\sigma_{(OH)(OH)}$ and $\sigma_{(OH)(Ow)}$ to reach similar densities as shown in Figure 2a. Despite the accurate density predictions of all force fields, the viscosities of the V1−V4 force fields differ by more than 50 %. As shown in Figure 2b, reducing the absolute value of the charge on $(OH)^-$ ($q_{(OH)}$) (comparison between V1, V2, and V4) and/or the total charge on $B(OH)_4^-$ ($q_{B(OH)_4}$) (comparison between V3 and V4) leads to lower viscosities. The densities and viscosities of the EPSR $NaB(OH)_4$ force field of Zhou et al.[20] (assuming a rigid structure for $B(OH)_4^-$) in TIP4P/2005 water[46] are computed as a comparison. Both the density (1240 ± 1 kg/m^3) and viscosity (4.3±0.4 mPa s) of the rigid EPSR force field[20] at 5 mol $NaB(OH)_4$/kg water and 298 K are underpredicted compared to experimental values by ca. 2.5 and 26%, respectively. Despite being rather accurate for the density, the viscosity computed at 5 mol $NaB(OH)_4$/kg water using the EPSR force field[20] is an order of magnitude

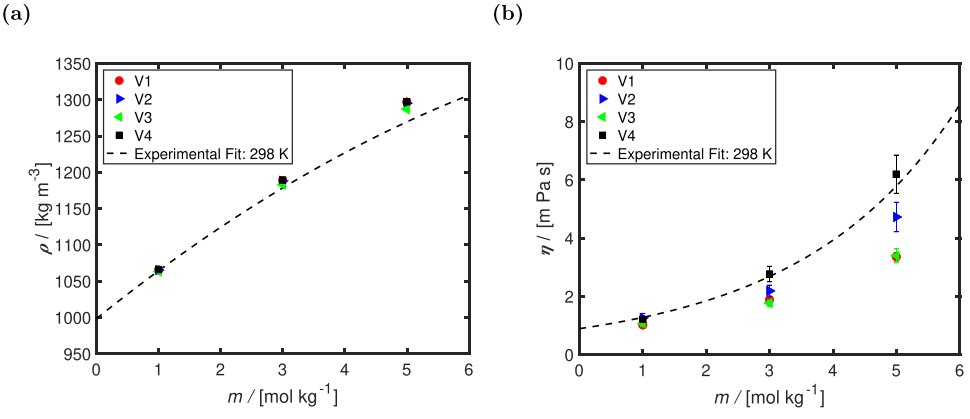

Figure 2. Computed (a) densities (ρ) and (b) viscosities (η) as functions of $NaB(OH)_4$ molality (m) at 298 K and 1 bar. The V1−V4 models (details in Table 1) are combined with TIP4P/2005 water,[46] and the Madrid-2019[47] and the Madrid-Transport[56] Na^+ force fields. The experimental correlation for densities and viscosities of Zhou et al.[21] are shown as dashed lines.

https://doi.org/10.1021/acs.iecr.3c01422
Ind. Eng. Chem. Res. 2023, 62, 11992−12005

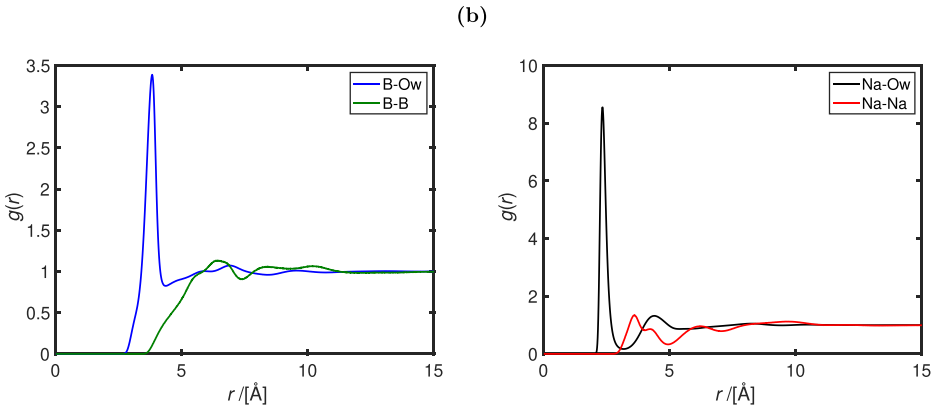

Figure 3. Radial distribution functions ($g(r)$) for (a) $B(B(OH)_4^-)-O_w$ (O of water) and $B(B(OH)_4^-)-B(B(OH)_4^-)$, and (b) $Na^+ - O_w$ and $Na^+ - Na^+$, as a function of radial distance r (Å), at 298 K, 1 bar, and a concentration of 5 mol $NaB(OH)_4$/kg water. The DFF/$B(OH)_4^-$ is used and combined with the TIP4P/2005[46] water and Madrid-2019[47] Na^+ force fields.

more inaccurate compared to the viscosities computed using the V4 force field of $B(OH)_4^-$.

Overall, the V4 force field with a charge scaling of 0.85 leads to optimal agreement with experimentally measured viscosities at 298 K (within 2% deviation). Zeron et al.[47] have also shown that by applying a charge scaling of 0.85, the viscosities of Na_2SO_4 and K_2SO_4 can be computed accurately (less than 1% deviation from experiments). The recent work by Blazquez et al.[56] and Habibi et al.[41] has shown that the 0.75 charge scaling is optimal for computing the viscosities of aqueous NaCl, KCl, NaOH, and KOH solutions. This indicates that there is a different optimal charge scaling for computing viscosities of electrolyte solutions, depending on the system. Since the V4 force field has the best agreement with experimental densities and viscosities, the final parameters of the DFF/$B(OH)_4^-$ are the ones of V4 (see Table 1). We have carried out an additional transferability check for DFF/$B(OH)_4^-$ with a recent modification of TIP4P/2005 developed by Rahbari et al.[94] (denoted here as TIP4P/μ) shown in Figure S2 of the Supporting Information. Although TIP4P/2005 can accurately model the densities and transport properties of water, it is less accurate in capturing properties such as the experimental saturated vapor pressures.[46,53,94] TIP4P/μ[94] can accurately model the saturated vapor pressures of water despite having less accurate predictions for the liquid viscosities compared to TIP4P/2005.[46] As shown in Figure S2, the combination of DFF/$B(OH)_4^-$ with TIP4P/μ results in accurate densities (maximum deviation of 2%) for aqueous $NaB(OH)_4^-$ solutions.

The radial distribution functions (RDF: $g(r)$) for B (B of $B(OH)_4^-$)$-O_w$ (O of water), B−B, $Na^+ - O_w$, and $Na^+ - Na^+$ are shown in Figure 3. The first RDF peak for $B-O_w$ is at ca. 3.80 Å (Figure 3a). For $Na^+ - O_w$, the first peak at 2.31 Å is found (Figure 3b). These results agree with the atomistic simulations of aqueous $NaB(OH)_4$ of Zhou et al.[20] The authors indicated the first peak of 3.72 and 2.34 Å for $B-O_w$ and $Na^+ - O_w$, respectively. The first hydration number (n_{hyd}) of B and Na^+ can be computed from[41,47]

$$n_{hyd} = 4\pi\langle\rho_w\rangle \int_0^{r_{min}} g_w(r) r^2 dr \quad (10)$$

where $\langle\rho_w\rangle$ is the average number density of water molecules, r is the radial distance, $g_w(r)$ is the RDF of either B or Na^+ with O_w, and r_{min} is the first minimum of $g_w(r)$. The computed hydration numbers of B and Na^+ at 5 mol $NaB(OH)_4$ are 10.9 and 5.6, respectively. Zhou et al.[20] report hydration numbers in the ranges from 12.9−15.6 to 3.7−5.4 for B and Na^+, respectively. A prior diffraction study of aqueous $NaB(OH)_4$ solutions by Zhou et al.[95] reports hydration numbers in the ranges from 6 to 12 and 5.8 to 6.0 for B and Na^+, respectively. In general, the location of the computed first peaks for RDFs of $B-O_w$ and $Na^+ - O_w$ is in excellent agreement with previous works in the literature,[20,95] while a reasonable agreement is found for the hydration numbers of B and Na^+.[20,95] These results for the structure of aqueous $NaB(OH)_4$ indicate that the hydrodynamic radius of the $B(OH)_4^-$ and Na^+ is modeled reasonably and that no crystallization occurred during the MD simulations.

From this section onwards, the DFF/$B(OH)_4^-$ (version V4 of Table 1) is used to compute densities, transport properties (e.g., viscosities and electrical conductivities), solubilities of H_2, and activities of water in aqueous $NaB(OH)_4$ solutions. The $B(OH)_4^-$ model developed in this work may also be used to study other systems such as aqueous $KB(OH)_4$ or $LiB(OH)_4$ systems as K^+ and Li^+ force fields have been developed in Madrid-2019.[47] Studying the performance of the $B(OH)_4^-$ force field for different cations is beyond the scope of this work.

3.2. Temperature Dependence of Viscosities and Densities. Figure 4 shows the temperature dependence of computed densities and viscosities of aqueous $NaB(OH)_4$ solutions at different molalities of $NaB(OH)_4$. The densities and viscosities shown in Figure 4 are computed from MD simulations using the DFF/$B(OH)_4^-$ of $B(OH)_4^-$, the TIP4P/2005 water force field,[46] and the Madrid-2019 Na^+ force field.[47] The experimental data of Zhou et al.[21] at 298 and 323 K are also plotted in Figure 4. As shown in Figure 4a, the computed densities in this work are in excellent agreement (within 2.5% deviation) with the experimental results of Zhou et al.[21] for both temperatures. The viscosities computed in this work at 298, 323, 333, 343, and 353 K are fitted to an empirical correlation of the form:

$$\eta = \eta_0 \exp\left[A_1 m + \frac{A_2}{T}\right] \quad (11)$$

where η_0, A_1, and A_2 are fitting constants. The values of these fitting constants are listed in Table 2. The results of this empirical correlation are shown as solid lines in Figure 4b,c. The viscosity of pure water as a function of temperature is

https://doi.org/10.1021/acs.iecr.3c01422
Ind. Eng. Chem. Res. 2023, 62, 11992−12005

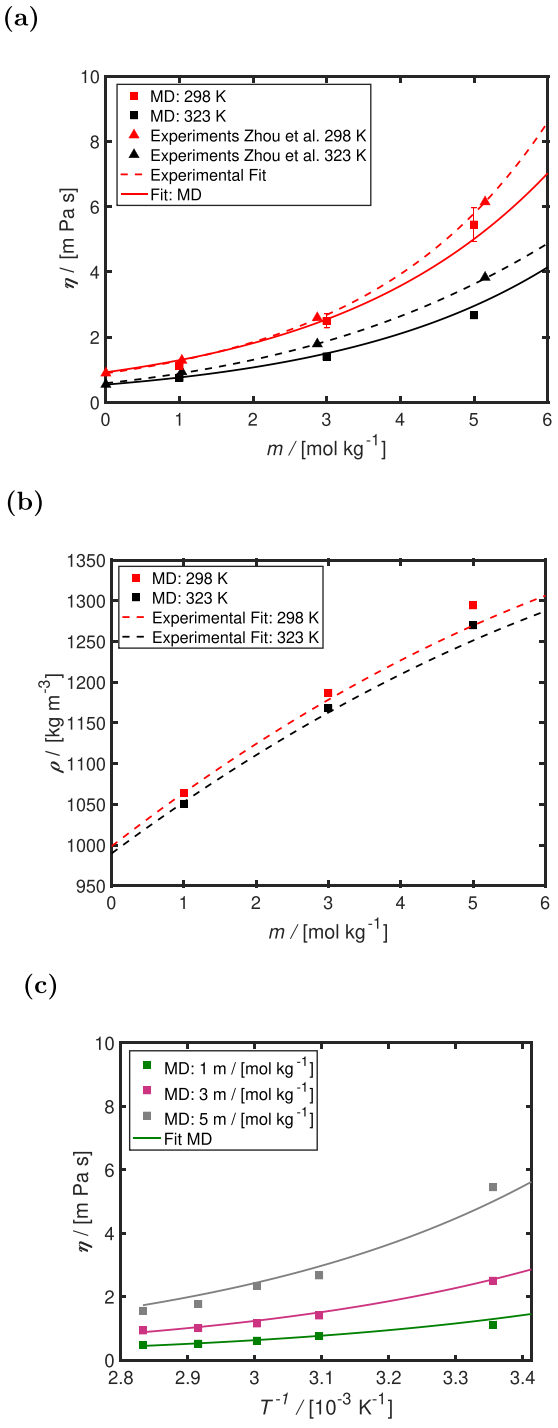

Figure 4. Computed (a) densities (ρ) and (b) viscosities (η) as functions of molality m in units of mol $NaB(OH)_4$/kg water at 298 and 323 K at 1 bar. In (c), η is shown as a function of the reciprocal temperature (T^{-1}) at 1, 3, and 5 m at 1 bar. The experimental densities and viscosities of Zhou et al.[21] at 298 and 323 K are shown in (a) and (b). The dashed lines are the experimental fits for densities and viscosities based on the results of Zhou et al.[21] The solid lines represent eq 11 based on the parameters shown in Table 2. The densities and viscosities are computed from MD simulations using the DFF/$B(OH)_4^-$ combined with the TIP4P/2005[46] water and Madrid-2019[47] Na^+ force fields.

reproduced using eq 11 with a maximum deviation of 10% for a temperature range of 298−353 K as shown in Figure S3 of the Supporting Information.

Table 2. Parameters of Eq 11 for the Computed Viscosities of Aqueous $NaB(OH)_4$ Solutions[a]

η_0/[mPa s]	1.018×10^{-3}
A_1/[$(mol_{NaB(OH)_4}/ kg_{H_2O})^{-1}$]	3.379×10^{-1}
A_2/[K]	2.030×10^{3}

[a]The viscosities are computed from MD simulations using the DFF/$B(OH)_4^-$ combined with the TIP4P/2005[46] water and Madrid-2019[47] Na^+ force fields. These parameters are valid at a concentration range of 0−5 mol $NaB(OH)_4$ /kg water at 298−353 K.

As shown in Figure 4b, the computed viscosities at 323 K agree with the results of Zhou et al.[21] The viscosities deviate by 2% up to a molality of 3 mol $NaB(OH)_4$/kg water, and by ca. 10% at a molality of 5 mol $NaB(OH)_4$/kg water at 323 K. Overall, it can be concluded that the MD simulations can accurately model both the densities and viscosities at 323 K even though the $B(OH)_4^-$ force field is only fitted to data at 298 K. In Figure 4c, an exponential increase in the viscosities is observed as a function of the reciprocal temperature ($\eta \propto \exp[A_2/T]$). This behavior has also been observed in other experimental and simulation studies of aqueous electrolyte solutions (e.g., NaCl and NaOH).[40,41,96,97]

3.3. Electrical Conductivities and Self-Diffusivities of Ions. The computed electrical conductivities of aqueous $NaB(OH)_4$ solutions are shown in Figure 5a,b. The finite-size corrected[70,71,98] self-diffusivities of Na^+ and $B(OH)_4^-$ in aqueous $NaB(OH)_4$ solutions are shown in Figure 5c,d, respectively. The computed finite-size corrected self-diffusivities (D_s) of Na^+ and $B(OH)_4^-$ are fitted to an empirical function with a functional form of

$$D_s = D_{s,0}\exp\left[-B_1 m - \frac{B_2}{T}\right] \quad (12)$$

where $D_{s,0}$, B_1, and B_2 are fitting constants. m is the molality of $NaB(OH)_4$ in units of mol $NaB(OH)_4$/kg water, and T is in units of K. The values of these fitting constants for Na^+ and $B(OH)_4^-$ are listed in Table 3. The results of the fitting equation are shown in Figure 5c,d as solid lines. The experimentally measured infinite dilution diffusion coefficients at 298 K for Na^+ and $B(OH)_4^-$ are 1.33×10^{-9} m^2/s and 0.96×10^{-9} m^2/s, respectively.[20,47] The infinite dilution self-diffusivities at 298 K obtained in this work by fitting the computed self-diffusivities ($D_{s,0}$) for Na^+ and $B(OH)_4^-$ are 1.2×10^{-9} m^2/s and 0.94×10^{-9} m^2/s, respectively. The computed (finite-size corrected[70,71]) self-diffusivities of Na^+ and $B(OH)_4^-$ at a molality of 0.5 mol $NaB(OH)_4$/kg water and 298 K are $(1.13 \pm 0.03) \times 10^{-9}$ m^2/s and $(0.85 \pm 0.06) \times 10^{-9}$ m^2/s, respectively. These values are in agreement with the values predicted from eq 12 and the experimentally measured infinite dilution diffusion coefficients for Na^+ and $B(OH)_4^-$ in water.[20,47]

In Figure 5a, the electrical conductivities at 298 K computed using the NE approximation (eq 3) and the exact expression (eq 1) are compared to the experimental results of Zhou et al.[21] Consistent with what is found for other aqueous electrolyte solutions,[76,81] the NE equation overestimates electrical conductivities with respect to the exact expression (eq 1). The ion−ion correlations, which are ignored in the NE approximation and accounted for in the exact expression, lower the electrical conductivities and play an important role in accurate predictions of electrical conductivities.[81] This is also observed in the literature for other systems such as aqueous

https://doi.org/10.1021/acs.iecr.3c01422
Ind. Eng. Chem. Res. 2023, 62, 11992−12005

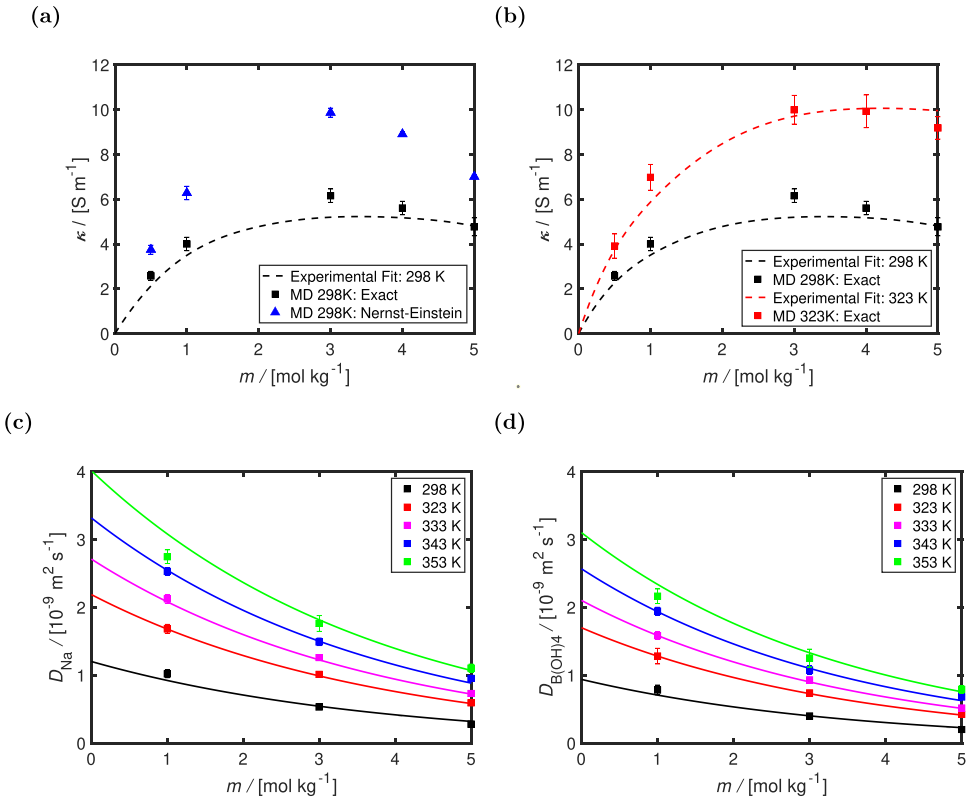

Figure 5. Computed electrical conductivities of aqueous $NaB(OH)_4$ as functions of $NaB(OH)_4$ molality (m) are shown in (a) and (b). In (a), the electrical conductivities computed using the exact (eq 1) and the Nernst−Einstein (eq 3) equation at 298 K and 1 bar are shown. The self-diffusivities of ions used in the Nernst−Einstein equation (eq 3) are corrected for finite-size effects using the Yeh−Hummer correction.[70,71] In (b), the computed exact electrical conductivities (eq 1) are shown at 298 and 323 K. The experimental fit of Zhou et al.[21] for electrical conductivities at 298 and 323 K is shown in (a) and (b) as dashed lines. The computed finite-size corrected self-diffusivities of (c) Na^+ (D_{Na}) and (d) $B(OH)_4^-$ ($D_{B(OH)_4}$) are shown as functions of m at 1 bar and different temperatures (298−353 K). The solid lines represent eq 12 with the fitting parameters listed in Table 3. The DFF/$B(OH)_4^-$ is used and combined with the TIP4P/2005[46] water and Madrid-2019[47] Na^+ force fields.

Table 3. Parameters of Eq 12 for the Computed Finite-Size Corrected Self-Diffusivities of Na^+ and $B(OH)_4^-$ in Aqueous $NaB(OH)_4$ Solutions[a]

	$B(OH)_4^-$	Na^+
$D_{s,0}/[m^2/s]$	1.998×10^{-6}	2.736×10^{-6}
$B_1/[(mol_{NaB(OH)_4}/kg_{H_2O})^{-1}]$	2.820×10^{-1}	2.642×10^{-1}
$B_2/[K]$	2.283×10^{3}	2.303×10^{3}

[a]The finite-size corrected self-diffusivities are computed from MD simulations using the DFF/$B(OH)_4^-$ combined with the TIP4P/2005[46] water and Madrid-2019[47] Na^+ force fields. These parameters are valid at a concentration range of 0−5 mol $NaB(OH)_4$ /kg water at 298−353 K.

NaCl.[76,81] At the limit of low $NaB(OH)_4$ molalities ($m \to 0$), the NE expression and the exact expression (eq 1) are identical by definition. This is (by definition) not the case for exact expression (eq 1) and the NE expression with the Yeh−Hummer correction[70,71] ionic diffusivities. At the limit of low $NaB(OH)_4$ molalities ($m \to 0$), the exact expression (eq 1) is expected to have the same finite-size effects as the NE expression without the Yeh−Hummer corrected diffusivities. As shown in Figure S4 and briefly discussed in its caption, the finite-size effects of the exact electrical conductivities (for m larger than zero) are within the error bars of the values computed with MD simulations (ca. 10%). Thus, no definite conclusion regarding the precise magnitude of these finite-size effects can be made here. We feel that the derivation of an analytic expression for correcting the finite-size effects of electrical conductivities computed using eq 1 is beyond the scope of this work.

In Figure 5b, the exact electrical conductivities (eq 1) at 298 and 323 K are compared to the experimental results of Zhou et al.[21] At both temperatures, the computed electrical conductivities initially increase as a function of salt molality and then decline at higher concentrations. The initial increase in electrical conductivities is due to the increase in the number of charge carriers, while the subsequent decline is attributed to the increase in the viscosity (and decrease in ion diffusivities) at higher salt molalities.[76] This behavior has also been observed for other electrolyte solutions.[99,100] The decrease in the self-diffusivities of Na^+ and $B(OH)_4^-$ as a function of salt molality can be observed in Figure 5c,d, respectively. Overall, the infinite dilution diffusivities of the ions and the electrical conductivities (and their temperature variations) are accurately modeled by the newly fitted DFF/$B(OH)_4^-$ developed here despite the force field being trained only on densities, viscosities, and RDF data.

3.4. Self-Diffusivities of H_2 in Aqueous $NaB(OH)_4$ Solutions. The computed self-diffusivities of H_2 (D_{H_2}) in aqueous $NaB(OH)_4$ solutions are shown in Figure 6. To the best of our knowledge, no experimental data are available for diffusivities of H_2 in aqueous $NaB(OH)_4$ solutions. Therefore, our simulations are the first predictions of this property. Similar to the self-diffusivities of Na^+ and $B(OH)_4^-$, the self-

https://doi.org/10.1021/acs.iecr.3c01422
Ind. Eng. Chem. Res. 2023, 62, 11992−12005

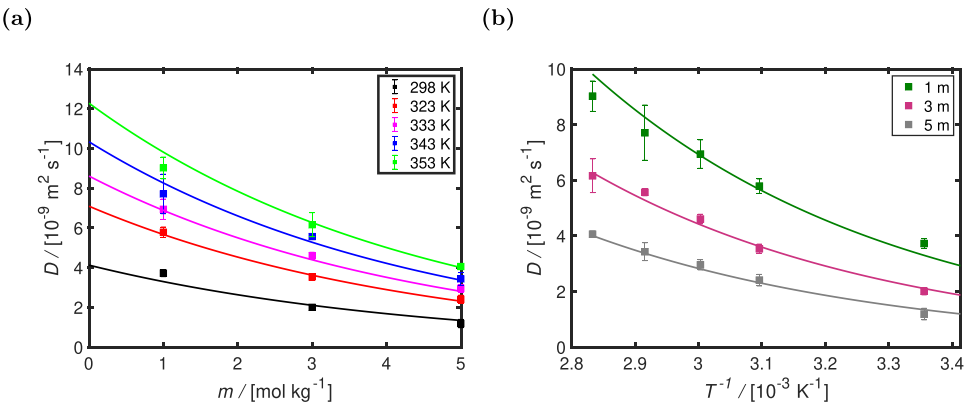

Figure 6. Self-diffusivities (D) of H_2 as a function of (a) $NaB(OH)_4$ molality (m in mol $NaB(OH)_4$/kg water) and (b) reciprocal of temperature (T^{-1} in K^{-1}). The DFF/$B(OH)_4^-$ is used and combined with the TIP4P/2005[46] water, Madrid-2019[47] Na^+, and the Marx[58] H_2 force fields. All self-diffusivities are corrected for finite-size effects using the Yeh−Hummer equation.[70,71]

diffusivities of H_2 are fitted to eq 12. The fitting constants of eq 12 for the self-diffusivities of H_2 are listed in Table 4. This

Table 4. Parameters of Eq 12 for the Computed Finite-Size Corrected Self-Diffusivities of H_2 in Aqueous $NaB(OH)_4$ Solutions[a]

$D_{s,0}/[m^2/s]$	4.503×10^{-6}
$B_1/[(mol_{NaB(OH)_4}/kg_{H_2O})^{-1}]$	2.240×10^{-1}
$B_2/[K]$	2.084×10^{3}

[a]The finite-size corrected self-diffusivities of H_2 are computed from MD simulations using the DFF/$B(OH)_4^-$ combined with the TIP4P/2005[46] water, Madrid-2019[47] Na^+, and Marx[58] H_2 force fields. These parameters are valid for a concentration range of 0−5 mol $NaB(OH)_4$/kg water at 298−353 K.

empirical correlation has also been used to model the self-diffusivities of H_2 in aqueous NaCl solutions[40] for a wide range of temperatures (298−523 K) and concentrations (0−6 mol NaCl/kg water).

In Figure 6a, an exponential decay of the self-diffusivities of H_2 as a function of $NaB(OH)_4$ molalities is observed. This is consistent with the increase of viscosities as a function of $NaB(OH)_4$ molalities as the self-diffusivities of gasses and viscosities of the solution are inversely related.[40,41] As shown in Figure 6b, the self-diffusivities of H_2 have an Arrhenius relation with respect to the temperature ($D_{H_2} \propto \exp[-A/T]$). These findings are consistent with other simulations and experiments for gas diffusion in aqueous solutions.[40,41]

3.5. Solubilities of H_2 and Activities of Water in Aqueous $NaB(OH)_4$ Solutions. Figure 7 shows the computed solubilities of H_2 and activities of water in aqueous $NaB(OH)_4$ solutions at 1 bar. The ratio between the solubilities of H_2 (expressed as a mole fraction) in the aqueous solution over the computed solubility in pure water ($x_{H_2}/x_{H_2,0}$) is plotted as a function of $NaB(OH)_4$ concentration in Figure 7a. The reduction of H_2 solubilities in aqueous solutions due to addition of salts (i.e., salting-out effect) is a well-established phenomenon.[40,41,101] To the best of our knowledge, no experimental data are available for the solubilities of H_2 in aqueous $NaB(OH)_4$ solutions. The salting-out of H_2 in aqueous solutions is commonly modeled using the Sechenov relation.[101] The Sechenov relation and constants provided by Weisenberger and Schumpe[101] are used in this work to compute $x_{H_2}/x_{H_2,0}$ for aqueous NaCl, NaI, $NaNO_3$, and $NaClO_4$ as shown in Figure 7a. Similarly to $B(OH)_4^-$, Cl^-, I^-, NO_3^-, and ClO_4^- are monovalent and do not have a dipole moment. The computed salting out of H_2 in aqueous $NaB(OH)_4$ solutions shown in Figure 7a is in qualitative agreement with other aqueous electrolyte solutions and in quantitative agreement with the salting out of H_2 in aqueous NaCl solutions.

All the computed solubilities of H_2 (x_{H_2}) at a H_2 partial pressure of 1 bar (298, 323, and 353 K) are fitted to an empirical equation inspired by the Sechenov relation:[101]

$$\ln\left[\frac{x_{H_2}}{x_{H_2,0}}\right] = (f_0 + f_1 T)m \tag{13}$$

where f_0 and f_1 are fitting constants. m is the molality of $NaB(OH)_4$ in units of mol $NaB(OH)_4$/kg water, and T is in units of K. $x_{H_2,0}$ is the computed solubility of H_2 in pure water at a H_2 partial pressure of 1 bar and is fitted to

$$x_{H_2,0} = f_2 \exp\left[\frac{f_3}{T} + f_4 \ln(T)\right] \tag{14}$$

where f_3, f_4, and f_5 are additional fitting parameters to capture the temperature dependence of H_2 solubilities in pure water. All the fitting constants for eqs 13 and 14 are shown in Table 5. Equation 14 is also used by Young[102] to model the experimental solubilities of H_2 in water. The computed solubilities of H_2 in water using the Marx H_2[58] force field and the TIP4P/2005[46] water force field underestimate experimental solubilities of H_2[102] by ca. 10%. The comparison of the experimental H_2 solubilities in water from 298 to 353 K with the solubility of Marx H_2 force field in the TIP4P/2005 water model is discussed in more detail in refs 40, 41. The results of eq 13 for the solubilities of H_2 in aqueous $NaB(OH)_4$ solutions at 298, 323, and 353 K are shown as solid lines in Figure 3c.

The computed activities of water in aqueous $NaB(OH)_4$ solutions at 298 and 353 K are compared to the activities of water in aqueous NaCl solutions (based on the activity correlation of Tang et al.[103]) in Figure 7c. It can be observed that the computed activities of water in this work are not strongly dependent on temperature. This is also observed in other works for activities of water (in the liquid phase) in

https://doi.org/10.1021/acs.iecr.3c01422
Ind. Eng. Chem. Res. 2023, 62, 11992−12005

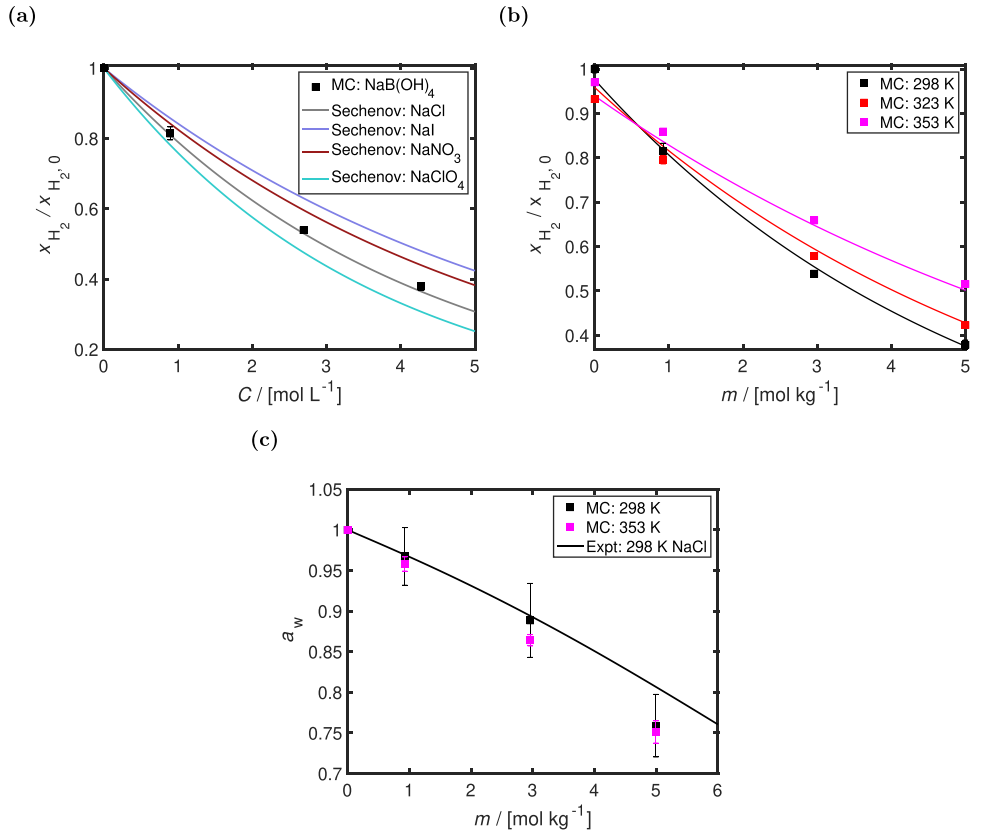

Figure 7. Computed (a,b) solubilities of H_2 and (c) activities of water (a_w) in aqueous $NaB(OH)_4$ solutions at a H_2 partial pressure of 1 bar. In (a), the mole fractions of H_2 (x_{H_2}) in the solution at 298 K divided by the computed H_2 solubility in pure water at 298 K ($x_{H_2,0}$), are shown as functions of concentration in units of mol salt/L solution. $x_{H_2}/x_{H_2,0}$ of H_2 in aqueous NaCl, NaI, $NaNO_3$, and $NaClO_4$ is plotted in (a) using the correlations provided by Weisenberger and Schumpe.[101] $x_{H_2}/x_{H_2,0}$ at 298, 323, and 353 K are shown as functions of molality (m) in units of mol salt/kg water in (b). The computed solubilities are fitted to an engineering equation (eq 13) and are shown as solid lines in (b). The DFF/$B(OH)_4^-$ is used and combined with the TIP4P/2005[46] water, Madrid-2019[47] Na^+, and the Marx[58] H_2 force fields. In (c), the computed activities of water (a_w) are plotted as a function of m at 298 and 353 K. The experimental activities of water at 298 K in aqueous NaCl solutions are plotted in (c) using the correlation provided by Tang et al.[103]

Table 5. Parameters of Eqs 13 and 14 for the Computed Solubilities of H_2 in Aqueous $NaB(OH)_4$ Solutions[a]

$f_0/[(\text{mol}_{NaB(OH)_4}/\text{kg}_{H_2O})^{-1}]$	-5.473×10^{-1}
$f_1/[(\text{K mol}_{NaB(OH)_4}/\text{kg}_{H_2O})^{-1}]$	1.195×10^{-3}
$f_2/[-]$	5.844×10^{-5}
$f_3/[\text{K}]$	-1.145×10^{1}
$f_4/[\ln(\text{K})^{-1}]$	-2.624×10^{-1}

[a]The solubilities of H_2 are computed from CFCMC simulations using the DFF/$B(OH)_4^-$ combined with the TIP4P/2005[46] water, Madrid-2019[47] Na^+, and Marx[58] H_2 force fields. These parameters are valid for a concentration range of 0−5 mol $NaB(OH)_4$ /kg water at 298−353 K.

aqueous NaCl solutions.[104] At lower salt molalities (below 3 mol salt/kg water), both $NaB(OH)_4^-$ and NaCl lead to similar changes to the water activities. At higher salt molalities (5 mol salt/kg water), the water activities start to deviate. Similar to the solubilities of H_2 , there are no experimental values for the activities of water in aqueous $NaB(OH)_4$ solutions. The values computed in this work can be used as the first estimate for this property to predict vapor pressures of water in aqueous $NaB(OH)_4$ solutions. All H_2 solubilities and activities of water at 298, 323, and 353 K computed in this work are shown in Table S7 of the Supporting Information.

4. CONCLUSIONS

In this work, the transport and thermodynamic properties of $H_2/H_2O/NaB(OH)_4$ mixtures are investigated. The Delft force field for $B(OH)_4^-$ (DFF/$B(OH)_4^-$) is proposed and parameterized based on TIP4P/2005 water[46] and the Madrid-2019[47] Na^+ force field. The combination of the DFF/$B(OH)_4^-$ with the Madrid-2019[47] Na^+ force field in TIP4P/2005[46] water can accurately predict the densities and viscosities of aqueous $NaB(OH)_4$ solutions up to the solubility limit at 298 K with 2.5% deviation from experimental results. These force fields are used to compute the viscosities, electrical conductivities, and self-diffusivities of H_2, Na^+, and $B(OH)_4^-$ for a concentration range of 0−5 mol $NaB(OH)_4$/kg water at 298−353 K and 1 bar. CFCMC simulations are used to compute the solubilities of H_2 and activities of water in $NaB(OH)_4$ solutions in the same temperature and concentration ranges as the MD simulations. The salting-out of H_2 in aqueous $NaB(OH)_4$ solutions is observed similar to the salting out of H_2 in other aqueous electrolyte solutions. The viscosities, self-diffusivities of the ions and H_2, and the solubilities of H_2 in aqueous $NaB(OH)_4$ solutions are fitted to engineering equations. These engineering equations can be used for modeling the crystallization of $NaB(OH)_4$ in the aqueous solution and for designing $NaBH_4$ hydrolysis reactors.

https://doi.org/10.1021/acs.iecr.3c01422
Ind. Eng. Chem. Res. 2023, 62, 11992−12005

We validated the performance of DFF/$B(OH)_4^-$ in combination with the TIP4P/μ[94] force field. Such a transferability check is important because although TIP4P/2005 can accurately model the densities and transport coefficients of water,[41] it is less accurate in capturing properties such as the experimental saturated vapor pressures.[94] When considering the vapor−liquid equilibrium of water/salt/H_2 systems, the hydrogen phase will contain a small amount of water. This can be accurately captured using TIP4P/μ.[94] In this work, we have shown that the combination of DFF/$B(OH)_4^-$ with TIP4P/μ[89] yields accurate predictions for experimental densities of aqueous $NaB(OH)_4$ solutions (maximum 2% deviation). A future outlook for expanding this work would be to validate the performance of DFF/$B(OH)_4^-$ for different cations (e.g., K^+) and in combination with other water force fields. Also, it would be interesting to investigate the exact magnitude of the finite-size effects of electrical conductivities using the exact expression (eq 1) in MD simulations.

■ ASSOCIATED CONTENT

Supporting Information

The Supporting Information is available free of charge at https://pubs.acs.org/doi/10.1021/acs.iecr.3c01422.

Force field parameters (Tables S1−S3); additional information on MD and CFCMC simulations (Tables S4 and S5); raw data of MD simulations for self-diffusivities (Table S6); raw data of CFCMC simulations (Table S7); densities of aqueous $NaB(OH)_4$ solutions using different $B(OH)_4^-$ force fields (Figure S1); densities of aqueous $NaB(OH)_4$ solutions using the TIP4P/μ force field of water (Figure S2); viscosities of pure water (Figure S3); and finite-size effects of computed electrical conductivities (Figure S4) (PDF)

Sample simulation files for MD and MC simulations in LAMMPS and BRICK-CFCMC software (ZIP)

■ AUTHOR INFORMATION

Corresponding Author

Othonas A. Moultos − *Engineering Thermodynamics, Process & Energy Department, Faculty of Mechanical Engineering, Delft University of Technology, 2628 CB Delft, The Netherlands;* orcid.org/0000-0001-7477-9684; Email: o.moultos@tudelft.nl

Authors

Parsa Habibi − *Engineering Thermodynamics, Process & Energy Department, Faculty of Mechanical Engineering, Delft University of Technology, 2628 CB Delft, The Netherlands; Department of Materials Science and Engineering, Faculty of Mechanical Engineering, Delft University of Technology, 2628 CD Delft, The Netherlands*

Julien R. T. Postma − *Complex Fluid Processing, Process & Energy Department, Faculty of Mechanical Engineering, Delft University of Technology, 2628 CB Delft, The Netherlands*

Johan T. Padding − *Complex Fluid Processing, Process & Energy Department, Faculty of Mechanical Engineering, Delft University of Technology, 2628 CB Delft, The Netherlands;* orcid.org/0000-0003-4161-0748

Poulumi Dey − *Department of Materials Science and Engineering, Faculty of Mechanical Engineering, Delft University of Technology, 2628 CD Delft, The Netherlands;* orcid.org/0000-0003-4679-1752

Thijs J. H. Vlugt − *Engineering Thermodynamics, Process & Energy Department, Faculty of Mechanical Engineering, Delft University of Technology, 2628 CB Delft, The Netherlands;* orcid.org/0000-0003-3059-8712

Complete contact information is available at: https://pubs.acs.org/10.1021/acs.iecr.3c01422

Notes

The authors declare no competing financial interest.

■ ACKNOWLEDGMENTS

This work was supported by the project SH2IPDRIVE: Sustainable Hydrogen Integrated Propulsion Drives, funded by the RVO under grant MOB21013. This work was sponsored by NWO Domain Science for the use of supercomputer facilities. O.A.M. gratefully acknowledges the support of NVIDIA Corporation with the donation of the Titan V GPU used for this research.

■ REFERENCES

(1) Gu, W.; Li, F.; Liu, X.; Gao, Q.; Gong, S.; Li, J.; Shi, S. Q. Borate chemistry inspired by cell walls converts soy protein into high-strength, antibacterial, flame-retardant adhesive. *Green Chem.* **2020**, *22*, 1319−1328.

(2) Li, B.; Ling, X.; Liu, X.; Li, Q.; Chen, W. Hydration of Portland cements in solutions containing high concentration of borate ions: Effects of LiOH. *Cem. Concr. Compos.* **2019**, *102*, 94−104.

(3) Xu, W.; Wang, X.; Wu, Y.; Li, W.; Chen, C. Functionalized graphene with Co-ZIF adsorbed borate ions as an effective flame retardant and smoke suppression agent for epoxy resin. *J. Hazard. Mater.* **2019**, *363*, 138−151.

(4) Stockmann, T. J.; Boyle, P. D.; Ding, Z. Preparation and crystal structure of tetraoctylphosphonium tetrakis(pentafluorophenyl)-borate ionic liquid for electrochemistry at its interface with water. *Catal. Today* **2017**, *295*, 89−94.

(5) Gulsoy, S. K.; Eroglu, H. Influence of Sodium Borohydride on Kraft Pulping of European Black Pine as a Digester Additive. *Ind. Eng. Chem. Res.* **2011**, *50*, 2441−2444.

(6) Ferguson, J. P.; Arcis, H.; Zimmerman, G. H.; Tremaine, P. R. Ion-Pair Formation Constants of Lithium Borate and Lithium Hydroxide under Pressurized Water Nuclear Reactor Coolant Conditions. *Ind. Eng. Chem. Res.* **2017**, *56*, 8121−8132.

(7) Van Hoecke, L.; Laffineur, L.; Campe, R.; Perreault, P.; Verbruggen, S. W.; Lenaerts, S. Challenges in the use of hydrogen for maritime applications. *Energy Environ. Sci.* **2021**, *14*, 815−843.

(8) Zhang, Q.; Wu, Y.; Sun, X.; Ortega, J. Kinetics of Catalytic Hydrolysis of Stabilized Sodium Borohydride Solutions. *Ind. Eng. Chem. Res.* **2007**, *46*, 1120−1124.

(9) Mosier-Boss, P. A.; Becker, C. A.; Anderson, G. W.; Wiedemeier, B. J. Feasibility Studies of the NaBH4/H2O Hydrolysis to Generate Hydrogen Gas to Inflate Lighter than Air (LTA) Vehicles. *Ind. Eng. Chem. Res.* **2015**, *54*, 7706−7714.

(10) Manoharan, K.; Palaniswamy, V. K.; Raman, K.; Sundaram, R. Investigation of solid state hydrogen storage performances of novel NaBH4/Ah-BN nanocomposite as hydrogen storage medium for fuel cell applications. *J. Alloys Compd.* **2021**, *860*, No. 158444.

(11) Tarhan, C.; Çil, M. A. A study on hydrogen, the clean energy of the future: Hydrogen storage methods. *J. Energy Storage* **2021**, *40*, No. 102676.

(12) Brack, P.; Dann, S. E.; Wijayantha, K. G. U. Heterogeneous and homogenous catalysts for hydrogen generation by hydrolysis of aqueous sodium borohydride (NaBH4) solutions. *Energy Sci. Eng.* **2015**, *3*, 174−188.

(13) Demirci, U. B.; Ouardia, A.; Andrieux, J.; Hannauer, J.; Chamoun, R.; Miele, P. Sodium borohydride hydrolysis as hydrogen

generator: issues, state of the art and applicability upstream from a fuel cell. *Fuel Cells* **2010**, *10*, 335.
(14) Zhang, Q.; Mohring, R. M. Reaction Chemistry Between Aqueous Sulfuric Acid and Solid Sodium Borohydride. *Ind. Eng. Chem. Res.* **2009**, *48*, 1603−1607.
(15) Marrero-Alfonso, E. Y.; Beaird, A. M.; Davis, T. A.; Matthews, M. A. Hydrogen Generation from Chemical Hydrides. *Ind. Eng. Chem. Res.* **2009**, *48*, 3703−3712.
(16) Hojjati-Najafabadi, A.; Aygun, A.; Tiri, R. N. E.; Gulbagca, F.; Lounissaa, M. I.; Feng, P.; Karimi, F.; Sen, F. Bacillus thuringiensis Based Ruthenium/Nickel Co-Doped Zinc as a Green Nanocatalyst: Enhanced Photocatalytic Activity, Mechanism, and Efficient H2 Production from Sodium Borohydride Methanolysis. *Ind. Eng. Chem. Res.* **2023**, *62*, 4655−4664.
(17) van Rheenen, E.; Padding, J.; Slootweg, C.; Visser, K. A review of the potential of hydrogen carriers for zero emission, low signature ship propulsion systems. 2021, http://library.imarest.org/record/10649 (accessed on Jun 30, 2023).
(18) Hung, A.-J.; Tsai, S.-F.; Hsu, Y.-Y.; Ku, J.-R.; Chen, Y.-H.; Yu, C.-C. Kinetics of sodium borohydride hydrolysis reaction for hydrogen generation. *Int. J. Hydrogen Energy* **2008**, *33*, 6205−6215.
(19) Beaird, A. M.; Li, P.; Marsh, H. S.; Al-Saidi, W. A.; Johnson, J. K.; Matthews, M. A.; Williams, C. T. Thermal Dehydration and Vibrational Spectra of Hydrated Sodium Metaborates. *Ind. Eng. Chem. Res.* **2011**, *50*, 7746−7752.
(20) Zhou, Y.; Higa, S.; Fang, C.; Fang, Y.; Zhang, W.; Yamaguchi, T. $B(OH)_4^-$ hydration and association in sodium metaborate solutions by X-ray diffraction and empirical potential structure refinement. *Phys. Chem. Chem. Phys.* **2017**, *19*, 27878−27887.
(21) Zhou, Y.; Fang, C.; Yang, Y.; Zhu, F. Volumetric and Transport Properties of Aqueous $NaB(OH)_4$ Solutions. *Chin. J. Chem. Eng.* **2013**, *21*, 1048−1056.
(22) Zhou, Y.; Fang, C.; Fang, Y.; Zhu, F. Polyborates in aqueous borate solution: A Raman and DFT theory investigation. *Spectrochim. Acta, Part A* **2011**, *83*, 82−87.
(23) Momii, R. K.; Nachtrieb, N. H. Nuclear magnetic resonance study of borate-polyborate equilibria in aqueous solution. *Inorg. Chem.* **1967**, *6*, 1189−1192.
(24) Lopalco, A.; Lopedota, A. A.; Laquintana, V.; Denora, N.; Stella, V. J. Boric Acid, a Lewis Acid With Unique and Unusual Properties: Formulation Implications. *J. Pharm. Sci.* **2020**, *109*, 2375−2386.
(25) Rustad, J. R.; Bylaska, E. J.; Jackson, V. E.; Dixon, D. A. Calculation of boron-isotope fractionation between $B(OH)_3$(aq) and $B(OH)_4$-(aq). *Geochim. Cosmochim. Acta* **2010**, *74*, 2843−2850.
(26) Perelygin, Y. P.; Chistyakov, D. Y. Boric acid. *Russ. J. Appl. Chem.* **2006**, *79*, 2041−2042.
(27) Applegarth, L. M. S. G. A.; Pye, C. C.; Cox, J. S.; Tremaine, P. R. Raman Spectroscopic and ab Initio Investigation of Aqueous Boric Acid, Borate, and Polyborate Speciation from 25 to 80 C. *Ind. Eng. Chem. Res.* **2017**, *56*, 13983−13996.
(28) Demirci, U. B.; Akdim, O.; Andrieux, J.; Hannauer, J.; Chamoun, R.; Miele, P. Sodium Borohydride Hydrolysis as Hydrogen Generator: Issues, State of the Art and Applicability Upstream from a Fuel Cell. *Fuel Cells* **2010**, *10*, 335−350.
(29) Demirci, U.; Akdim, O.; Miele, P. Ten-year efforts and a no-go recommendation for sodium borohydride for on-board automotive hydrogen storage. *Int. J. Hydrogen Energy* **2009**, *34*, 2638−2645.
(30) Atiyeh, H. K.; Davis, B. R. Separation of sodium metaborate from sodium borohydride using nanofiltration membranes for hydrogen storage application. *Int. J. Hydrogen Energy* **2007**, *32*, 229−236.
(31) Sousa, T.; Fernandes, V.; Pinto, P.; Slavkov, Y.; Bosukov, L.; Rangel, C. A sodium borohydride hydrogen generation reactor for stationary applications: Experimental and reactor simulation studies. *Chem. Eng. Sci.* **2012**, *84*, 70−79.
(32) Baye, A. F.; Abebe, M. W.; Appiah-Ntiamoah, R.; Kim, H. Engineered iron-carbon-cobalt (Fe_3O_4 C-Co) core-shell composite with synergistic catalytic properties towards hydrogen generation via $NaBH_4$ hydrolysis. *J. Colloid Interface Sci.* **2019**, *543*, 273−284.
(33) Yu, L.; Pellechia, P.; Matthews, M. A. Kinetic models of concentrated $NaBH_4$ hydrolysis. *Int. J. Hydrogen Energy* **2014**, *39*, 442−448.
(34) Liu, B.; Li, Z. Hydrogen generation from borohydride hydrolysis reaction. *J. Power Sources* **2009**, *187*, 527−534.
(35) Li, Q.; Kim, H. Hydrogen production from NaBH4 hydrolysis via Co-ZIF-9 catalyst. *Fuel Process. Technol.* **2012**, *100*, 43−48.
(36) Fernandes, V.; Pinto, A.; Rangel, C. Hydrogen production from sodium borohydride in methanol−water mixtures. *Int. J. Hydrogen Energy* **2010**, *35*, 9862−9868.
(37) Shabunya, S.; Minkina, V.; Kalinin, V.; Sankir, N.; Altaf, C. Kinetics of the catalytic hydrolysis of concentrated aqueous solutions of $NaBH_4$ on Co/TiO_2 powder. *Kinet. Catal.* **2021**, *62*, 350−359.
(38) Oronzio, R.; Monteleone, G.; Pozio, A.; De Francesco, M.; Galli, S. New reactor design for catalytic sodium borohydride hydrolysis. *Int. J. Hydrogen Energy* **2009**, *34*, 4555−4560.
(39) Liu, X.; Martín-Calvo, A.; McGarrity, E.; Schnell, S. K.; Calero, S.; Simon, J.-M.; Bedeaux, D.; Kjelstrup, S.; Bardow, A.; Vlugt, T. J. H. Fick Diffusion Coefficients in Ternary Liquid Systems from Equilibrium Molecular Dynamics Simulations. *Ind. Eng. Chem. Res.* **2012**, *51*, 10247−10258.
(40) van Rooijen, W. A.; Habibi, P.; Xu, K.; Dey, P.; Vlugt, T. J. H.; Hajibeygi, H.; Moultos, O. A. Interfacial Tensions, Solubilities, and Transport Properties of the H_2/H_2O/NaCl System: A Molecular Simulation Study. *J. Chem. Eng. Data* **2023**, DOI: 10.1021/acs.jced.2c00707. in press.
(41) Habibi, P.; Rahbari, A.; Blazquez, S.; Vega, C.; Dey, P.; Vlugt, T. J. H.; Moultos, O. A. A New Force Field for OH- for Computing Thermodynamic and Transport Properties of H_2 and O_2 in Aqueous NaOH and KOH Solutions. *J. Phys. Chem. B* **2022**, *126*, 9376−9387.
(42) Tsimpanogiannis, I. N.; Maity, S.; Celebi, A. T.; Moultos, O. A. Engineering Model for Predicting the Intradiffusion Coefficients of Hydrogen and Oxygen in Vapor, Liquid, and Supercritical Water based on Molecular Dynamics Simulations. *J. Chem. Eng. Data* **2021**, *66*, 3226−3244.
(43) Zhang, B.; Zhao, X.; Chen, Y.; Ge, Z.; Jin, H. Investigation of H2S Diffusion in Transcritical and Supercritical Water: A Molecular Dynamics Simulation Study. *Ind. Eng. Chem. Res.* **2023**, *62*, 3026−3037.
(44) Frenkel, D.; Smit, B. *Understanding molecular simulation: from algorithms to applications*, 2nd ed.; Elsevier: San Diego, 2002.
(45) Allen, M.; Tildesley, D.; Tildesley, D. *Computer Simulation of Liquids*, 2nd ed.; Oxford Science Publications; Oxford University Press: New York, 2017.
(46) Abascal, J. L.; Vega, C. A general purpose model for the condensed phases of water: TIP4P/2005. *J. Chem. Phys.* **2005**, *123*, 234505.
(47) Zeron, I. M.; Abascal, J. L. F.; Vega, C. A force field of Li^+, Na^+, K^+, Mg^{2+}, Ca^+, Cl^-, and SO_4^{2-} in aqueous solution based on the TIP4P/2005 water model and scaled charges for the ions. *J. Chem. Phys.* **2019**, *151*, 104501.
(48) Rahbari, A.; Hens, R.; Ramdin, M.; Moultos, O. A.; Dubbeldam, D.; Vlugt, T. J. H. Recent advances in the Continuous Fractional Component Monte Carlo methodology. *Mol. Simul.* **2021**, *47*, 804−823.
(49) Shi, W.; Maginn, E. J. Continuous Fractional Component Monte Carlo: an adaptive biasing method for open system atomistic simulations. *J. Chem. Theory Comput.* **2007**, *3*, 1451−1463.
(50) Shi, W.; Maginn, E. J. Improvement in molecule exchange efficiency in Gibbs ensemble Monte Carlo: Development and implementation of the Continuous Fractional Component move. *J. Comput. Chem.* **2008**, *29*, 2520−2530.
(51) Vega, C.; Abascal, J. L. Simulating water with rigid non-polarizable models: a general perspective. *Phys. Chem. Chem. Phys.* **2011**, *13*, 19663−19688.

(52) Vega, C.; Miguel, E. D. Surface tension of the most popular models of water by using the test-area simulation method. *J. Chem. Phys.* **2007**, *126*, 154707.
(53) Tsimpanogiannis, I. N.; Moultos, O. A.; Franco, L. F.; Spera, M. B. M.; Erdös, M.; Economou, I. G. Self-diffusion coefficient of bulk and confined water: a critical review of classical molecular simulation studies. *Mol. Simul.* **2019**, *45*, 425−453.
(54) Moultos, O. A.; Tsimpanogiannis, I. N.; Panagiotopoulos, A. Z.; Economou, I. G. Atomistic Molecular Dynamics Simulations of CO_2 Diffusivity in H_2O for a Wide Range of Temperatures and Pressures. *J. Phys. Chem. B* **2014**, *118*, 5532−5541.
(55) Döpke, M. F.; Moultos, O. A.; Hartkamp, R. On the transferability of ion parameters to the TIP4P/2005 water model using molecular dynamics simulations. *J. Chem. Phys.* **2020**, *152*, No. 024501.
(56) Blazquez, S.; Conde, M. M.; Vega, C. A. Scaled charges for ions: An improvement but not the final word for modeling electrolytes in water. *J. Chem. Phys.* **2023**, *158*, No. 054505.
(57) Panagiotopoulos, A. Z. Simulations of activities, solubilities, transport properties, and nucleation rates for aqueous electrolyte solutions. *J. Chem. Phys.* **2020**, *153*, No. 010903.
(58) Marx, D.; Nielaba, P. Path-integral Monte Carlo techniques for rotational motion in two dimensions: Quenched, annealed, and no-spin quantum-statistical averages. *Phys. Rev. A* **1992**, *45*, 8968.
(59) Plimpton, S. Fast parallel algorithms for short-range molecular dynamics. *J. Comput. Phys.* **1995**, *117*, 1−19.
(60) Nguyen, T. D.; Phillips, C. L.; Anderson, J. A.; Glotzer, S. C. Rigid body constraints realized in massively-parallel molecular dynamics on graphics processing units. *Comput. Phys. Commun.* **2011**, *182*, 2307−2313.
(61) Verlet, L. Computer "Experiments" on Classical Fluids. I. Thermodynamical Properties of Lennard-Jones molecules. *Phys. Rev.* **1967**, *159*, 98−103.
(62) Hockney, R. W.; Eastwood, J. W. *Computer simulation using particles*, 1st ed.; CRC Press: Boca Raton, 1988.
(63) Luty, B. A.; Davis, M. E.; Tironi, I. G.; Van Gunsteren, W. F. A comparison of particle-particle, particle-mesh and Ewald methods for calculating electrostatic interactions in periodic molecular systems. *Mol. Simul.* **1994**, *14*, 11−20.
(64) Pollock, E.; Glosli, J. Comments on P3M, FMM, and the Ewald method for large periodic Coulombic systems. *Comput. Phys. Commun.* **1996**, *95*, 93−110.
(65) Nosé, S. A Unified Formulation of the Constant Temperature Molecular Dynamics Methods. *J. Chem. Phys.* **1984**, *81*, 511−519.
(66) Hoover, W. G. Canonical Dynamics: Equilibrium Phase-Space Distributions. *Phys. Rev. A* **1985**, *31*, 1695.
(67) Kamberaj, H.; Low, R.; Neal, M. Time reversible and symplectic integrators for molecular dynamics simulations of rigid molecules. *J. Chem. Phys.* **2005**, *122*, 224114.
(68) Jamali, S. H.; Wolff, L.; Becker, T. M.; De Groen, M.; Ramdin, M.; Hartkamp, R.; Bardow, A.; Vlugt, T. J. H.; Moultos, O. A. OCTP: A tool for on-the-fly calculation of transport properties of fluids with the order-n algorithm in LAMMPS. *J. Chem. Inf. Model.* **2019**, *59*, 1290−1294.
(69) Jamali, S. H.; Wolff, L.; Becker, T. M.; Bardow, A.; Vlugt, T. J. H.; Moultos, O. A. Finite-Size Effects of Binary Mutual Diffusion Coefficients from Molecular Dynamics. *J. Chem. Theory Comput.* **2018**, *14*, 2667−2677.
(70) Yeh, I.-C.; Hummer, G. System-size dependence of diffusion coefficients and viscosities from molecular dynamics simulations with periodic boundary conditions. *J. Phys. Chem. B* **2004**, *108*, 15873−15879.
(71) Dünweg, B.; Kremer, K. Molecular dynamics simulation of a polymer chain in solution. *J. Chem. Phys.* **1993**, *99*, 6983−6997.
(72) Celebi, A. T.; Jamali, S. H.; Bardow, A.; Vlugt, T. J. H.; Moultos, O. A. Finite-size effects of diffusion coefficients computed from molecular dynamics: a review of what we have learned so far. *Mol. Simul.* **2021**, *47*, 831−845.
(73) Jamali, S. H.; Bardow, A.; Vlugt, T. J. H.; Moultos, O. A. Generalized form for finite-size corrections in mutual diffusion coefficients of multicomponent mixtures obtained from equilibrium molecular dynamics simulation. *J. Chem. Theory Comput.* **2020**, *16*, 3799−3806.
(74) Jamali, S. H.; Hartkamp, R.; Bardas, C.; Söhl, J.; Vlugt, T. J. H.; Moultos, O. A. Shear Viscosity Computed from the Finite-Size Effects of Self-Diffusivity in Equilibrium Molecular Dynamics. *J. Chem. Theory Comput.* **2018**, *14*, 5959−5968.
(75) Moultos, O. A.; Zhang, Y.; Tsimpanogiannis, I. N.; Economou, I. G.; Maginn, E. J. System-size corrections for self-diffusion coefficients calculated from molecular dynamics simulations: The case of CO_2, n-alkanes, and poly(ethylene glycol) dimethyl ethers. *J. Chem. Phys.* **2016**, *145*, 074109.
(76) Gullbrekken, Ø.; Røe, I. T.; Selbach, S. M.; Schnell, S. K. Charge Transport in Water−NaCl Electrolytes with Molecular Dynamics Simulations. *J. Phys. Chem. B* **2023**, *127*, 2729−2738.
(77) Schröder, C.; Haberler, M.; Steinhauser, O. On the computation and contribution of conductivity in molecular ionic liquids. *J. Chem. Phys.* **2008**, *128*, 134501.
(78) Onsager, L. Theories and Problems of Liquid Diffusion. *Ann. N. Y. Acad. Sci.* **1945**, *46*, 241−265.
(79) Krishna, R.; van Baten, J. M. The Darken Relation for Multicomponent Diffusion in Liquid Mixtures of Linear Alkanes: An Investigation Using Molecular Dynamics (MD) Simulations. *Ind. Eng. Chem. Res.* **2005**, *44*, 6939−6947.
(80) Krishna, R.; Wesselingh, J. The Maxwell-Stefan approach to mass transfer. *Chem. Eng. Sci.* **1997**, *52*, 861−911.
(81) Kubisiak, P.; Eilmes, A. Estimates of Electrical Conductivity from Molecular Dynamics Simulations: How to Invest the Computational Effort. *J. Phys. Chem. B* **2020**, *124*, 9680−9689.
(82) Martinez, L.; Andrade, R.; Birgin, E. G.; Martínez, J. M. PACKMOL: A package for building initial configurations for molecular dynamics simulations. *J. Comput. Chem.* **2009**, *30*, 2157−2164.
(83) Delft High Performance Computing Centre (DHPC) DelftBlue Supercomputer (Phase 1). 2022, https://www.tudelft.nl/dhpc/ark:/44463/DelftBluePhase1 (accessed on Jun 30, 2023).
(84) Hens, R.; Rahbari, A.; Caro-Ortiz, S.; Dawass, N.; Erdős, M.; Poursaeidesfahani, A.; Salehi, H. S.; Celebi, A. T.; Ramdin, M.; Moultos, O. A.; Dubbeldam, D.; Vlugt, T. J. H. Brick-CFCMC: Open Source Software for Monte Carlo Simulations of Phase and Reaction Equilibria Using the Continuous Fractional Component Method. *J. Chem. Inf. Model.* **2020**, *60*, 2678−2682.
(85) Polat, H. M.; Salehi, H. S.; Hens, R.; Wasik, D. O.; Rahbari, A.; de Meyer, F.; Houriez, C.; Coquelet, C.; Calero, S.; Dubbeldam, D.; Moultos, O. A.; Vlugt, T. J. H. New Features of the Open Source Monte Carlo Software Brick-CFCMC: Thermodynamic Integration and Hybrid Trial Moves. *J. Chem. Inf. Model.* **2021**, *61*, 3752−3757.
(86) Vörtler, H. L.; Schöfer, K.; Smith, W. R. Simulation of Chemical Potentials and Phase Equilibria in Two- and Three-Dimensional Square-Well Fluids: Finite Size Effects. *J. Phys. Chem. B* **2008**, *112*, 4656−4661.
(87) Wang, F.; Landau, D. P. Efficient multiple-range random walk algorithm to calculate the density of states. *Phys. Rev. Lett.* **2001**, *86*, 2050.
(88) Poulain, P.; Calvo, F.; Antoine, R.; Broyer, M.; Dugourd, P. Performances of Wang-Landau algorithms for continuous systems. *Phys. Rev. E* **2006**, *73*, No. 056704.
(89) Rahbari, A.; Brenkman, J.; Hens, R.; Ramdin, M.; Broeke, L. J. V. D.; Schoon, R.; Henkes, R.; Moultos, O. A.; Vlugt, T. J. H. Solubility of water in hydrogen at high pressures: A molecular simulation study. *J. Chem. Eng. Data* **2019**, *64*, 4103−4115.
(90) Hempel, S.; Fischer, J.; Paschek, D.; Sadowski, G. Activity coefficients of complex molecules by molecular simulation and Gibbs-Duhem integration. *Soft Mater.* **2012**, *10*, 26−41.
(91) Dubbeldam, D.; Calero, S.; Vlugt, T. J. H. iRASPA: GPU-accelerated visualization software for materials scientists. *Mol. Simul.* **2018**, *44*, 653−676.

https://doi.org/10.1021/acs.iecr.3c01422
Ind. Eng. Chem. Res. 2023, 62, 11992−12005

(92) Yamamoto, G.; Hirono, M. Rotational line width of methane. *J. Quant. Spectrosc. Radiat. Transfer* **1971**, *11*, 1537−1545.
(93) Birnbaum, G.; Cohen, E. R. Far infrared collision-induced absorption in gaseous methane. II. Determination of the octupole and hexadecapole moments. *J. Chem. Phys.* **1975**, *62*, 3807−3812.
(94) Rahbari, A.; Garcia-Navarro, J. C.; Ramdin, M.; van den Broeke, L. J. P.; Moultos, O. A.; Dubbeldam, D.; Vlugt, T. J. H. Effect of Water Content on Thermodynamic Properties of Compressed Hydrogen. *J. Chem. Eng. Data* **2021**, *66*, 2071−2087.
(95) Zhou, F.; Chunhui, Y.; Yan, F.; Fayan, Z.; Song, T.; Sha, X. Structure of aqueous sodium metaborate solutions: X-ray diffraction study. *Russ. J. Phys. Chem. A* **2012**, *86*, 1236−1244.
(96) Orozco, G. A.; Moultos, O. A.; Jiang, H.; Economou, I. G.; Panagiotopoulos, A. Z. Molecular simulation of thermodynamic and transport properties for the H_2O+NaCl system. *J. Chem. Phys.* **2014**, *141*, 234507.
(97) Jiang, H.; Mester, Z.; Moultos, O. A.; Economou, I. G.; Panagiotopoulos, A. Z. Thermodynamic and Transport Properties of H_2O + NaCl from Polarizable Force Fields. *J. Chem. Theory Comput.* **2015**, *11*, 3802−3810.
(98) Jamali, S. H.; Wolff, L.; Becker, T. M.; Bardow, A.; Vlugt, T. J. H.; Moultos, O. A. Finite-size effects of binary mutual diffusion coefficients from molecular dynamics. *J. Chem. Theory Comput.* **2018**, *14*, 2667−2677.
(99) Celebi, A. T.; Vlugt, T. J. H.; Moultos, O. A. Structural, Thermodynamic, and Transport Properties of Aqueous Reline and Ethaline Solutions from Molecular Dynamics Simulations. *J. Phys. Chem. B* **2019**, *123*, 11014−11025.
(100) Dawass, N.; Langeveld, J.; Ramdin, M.; Pérez-Gallent, E.; Villanueva, A. A.; Giling, E. J. M.; Langerak, J.; van den Broeke, L. J. P.; Vlugt, T. J. H.; Moultos, O. A. Solubilities and Transport Properties of CO_2, Oxalic Acid, and Formic Acid in Mixed Solvents Composed of Deep Eutectic Solvents, Methanol, and Propylene Carbonate. *J. Phys. Chem. B* **2022**, *126*, 3572−3584.
(101) Weisenberger, S.; Schumpe, A. Estimation of gas solubilities in salt solutions at temperatures from 273 K to 363 K. *AIChE J.* **1996**, *42*, 298−300.
(102) Young, C. L. *Solubility Data Series: Hydrogen and Deuterium*, 1st ed.; Pergamon Press: Oxford, 1981, Vol. *5/6*.
(103) Tang, I.; Munkelwitz, H.; Wang, N. Water activity measurements with single suspended droplets: The NaCl-H_2O and KCl-H_2O systems. *J. Colloid Interface Sci.* **1986**, *114*, 409−415.
(104) Reynolds, J. G. Salt Solubilities in Aqueous Solutions of NaNO3, NaNO2, NaCl, and NaOH: A Hofmeister-like Series for Understanding Alkaline Nuclear Waste. *ACS Omega* **2018**, *3*, 15149−15157.

https://doi.org/10.1021/acs.iecr.3c01422
Ind. Eng. Chem. Res. 2023, 62, 11992−12005